JOURNAL OF AIRCRAFT
Vol. 32, No. 2, March–April 1995

Aircraft with Single-Axis Aerodynamically Deployed Wings

Shlomo Djerassi* and Shmuel Kotzev†
RAFAEL, Ministry of Defense, Haifa 31021, Israel

This article deals with aircraft having two single-axis, aerodynamically deployed wings. Such aircraft are of current interest mainly in connection with unmanned drones. Two issues are discussed. The first relates to the formulation of equations governing the motion of the aircraft during and after the deployment, noting that imposition of constraints occurs when the deployment of each of the wings terminates. The second issue concerns choosing between two single axis configurations, called "up deployment" configuration and "low deployment" configuration, as better suited to carry out a successful deployment. It is shown that to obtain meaningful predictions of the dynamical behavior of the aircraft, one has to invoke the theory of imposition of constraints, excluding alternate theories as leading to time-consuming, inaccurate simulations; and that low deployment configuration is less susceptible to external winds during deployment, and therefore, superior to the up deployment configuration.

Introduction

AIRCRAFT with deployable wings are of increasing interest, because they occupy minimal space in storage, a useful feature that can be exploited, as, e.g., in unmanned aircraft. A variety of ideas were developed in connection with the realization of such aircraft,[1–7] two of which represent actual products (MBB's DAR[4] and Boeing's Brave-200[5]). A great deal of attention was paid to the deployment process, especially to the number, location, and orientation of the axes about which deployment occurs, to the power source energizing the deployment, and to the timing and synchronization of the deployment of the various wings. For example, Refs. 1–6 suggest a single-axis deployment for small, unmanned aircraft, whereas Ref. 7 discusses a two-axes deployment for a large, cruise ballistic missile. References 3 and 7 (first axis) mention transmission actuated wings, Ref. 4 considers spring actuated wings, Ref. 6 speaks about rods actuated wings, and Refs. 1, 2, and 7 (second axis) propose aerodynamically deployed wings. Axes parallel to the centerline of the aircraft are used in Refs. 1 and 4; axes perpendicular to the centerline of the aircraft are used in Refs. 3, 5, and 7 (first axis); and tilted axes are introduced by Refs. 1, 2, and 6. With the exception of Ref. 5, all the other references speak about deployment after launch. In Refs. 3, 6, and 7 (first axis) two (four in Ref. 6) wings are deployed simultaneously. Finally, the wings in Refs. 4 and 7 are provided with passive dampers. Whereas the indicated references are by no means exhaustive, they clearly indicate an area of current interest.

A particularly unique design is the one described in Refs. 1 and 2, based on single-axis, aerodynamically deployed wings. Aircraft with such wings are simple in structure, and need no power source in addition to the ones required for launch and flight. They also carry the potential of enhancing the deployment using their forward acceleration during launch. The wings can be deployed upon launch and, within limits, can be designed so that each will deploy independently of the others. It is this kind of aircraft with which the present work is concerned.

Received June 10, 1993; presented as Paper 93-3673 at the AIAA Atmospheric Flight Mechanics Conference, Monterey, CA, Aug. 9–11, 1993; revision received Feb. 25, 1994; accepted for publication May 19, 1994. Copyright © 1994 by S. Djerassi and S. Kotzev. Published by the American Institute of Aeronautics and Astronautics, Inc., with permission.

*Chief R&D Engineer, Ph.D., P.O. Box 2250.
†R&D Engineer, P.O. Box 2250.

Figure 1 depicts a model of an aircraft system S, consisting of a fuselage A and of wings B and C in stored configuration (Fig. 1a), and in fully deployed configuration (Fig. 1b). The following question is related to the transition between the two configurations. Is there an axis fixed in both B and A, and an angle θ, such that, if B is rotated about the indicated axis relative to A an amount θ, starting with the configuration shown in Fig. 1a, then B ends up having the configuration shown in Fig. 1b? One can show, with the aid of Ref. 8, Sec. 1.1, that, in fact, two such axes exist, each parallel to one of the following unit vectors:

$$\boldsymbol{\lambda}_{BU} = (1/\sqrt{3})(-\boldsymbol{b}_1 - \boldsymbol{b}_2 - \boldsymbol{b}_3) \tag{1}$$

$$\boldsymbol{\lambda}_{BL} = (1/\sqrt{3})(-\boldsymbol{b}_1 - \boldsymbol{b}_2 + \boldsymbol{b}_3) \tag{2}$$

and that

$$\theta = 120 \text{ deg} \tag{3}$$

Here, $\boldsymbol{b}_i$, and similarly, $\boldsymbol{a}_i$, $\boldsymbol{c}_i$, and $\boldsymbol{n}_i$ ($i = 1, 2, 3$), are sets of three dextral, mutually perpendicular unit vectors, fixed in B, A, C, and N, a Newtonian reference frame, respectively, directed as shown in Fig. 1.

Similar results can be obtained in connection with C, viz.,

$$\boldsymbol{\lambda}_{CU} = (1/\sqrt{3})(-\boldsymbol{c}_1 - \boldsymbol{c}_2 + \boldsymbol{c}_3) \tag{4}$$

$$\boldsymbol{\lambda}_{CL} = (1/\sqrt{3})(-\boldsymbol{c}_1 - \boldsymbol{c}_2 - \boldsymbol{c}_3) \tag{5}$$

and θ is as in Eq. (3). Configurations, as in Fig. 1, with deployment axes parallel to $\boldsymbol{\lambda}_{BU}$ and $\boldsymbol{\lambda}_{CU}$ in Eqs. (1) and (4) are called up deployment, or UD configurations; and configurations, as in Fig. 2, with deployment axes parallel to $\boldsymbol{\lambda}_{BL}$ and $\boldsymbol{\lambda}_{CL}$ in Eqs. (2) and (5) are called low deployment, or LD configurations. Snapshots of the UD and the LD configurations during deployment are shown in Figs. 1d and 2d, respectively.

Suppose A^*, the mass center of A, has been imparted an initial velocity, and that, when released, B and C are acted upon by springs exerting torques about their respective axes, directed such that B and C are forced into the airstream surrounding the fuselage. Then aerodynamic forces and torques are exerted on B and C, and these provide the power required to carry out the deployment.

Questions such as the following arise in connection with the aircraft under consideration. Which of the configurations is better suited for successful completion of the deployment? How do external winds affect the deployment process? To answer such questions one needs analytical tools, i.e., equa-

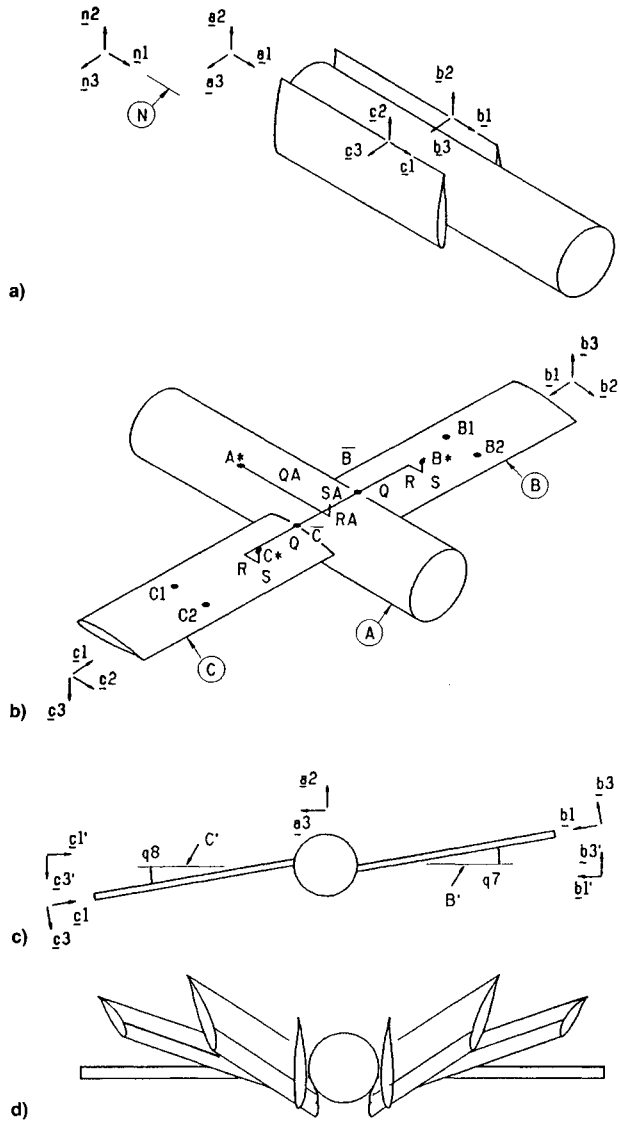

Fig. 1 UD configuration.

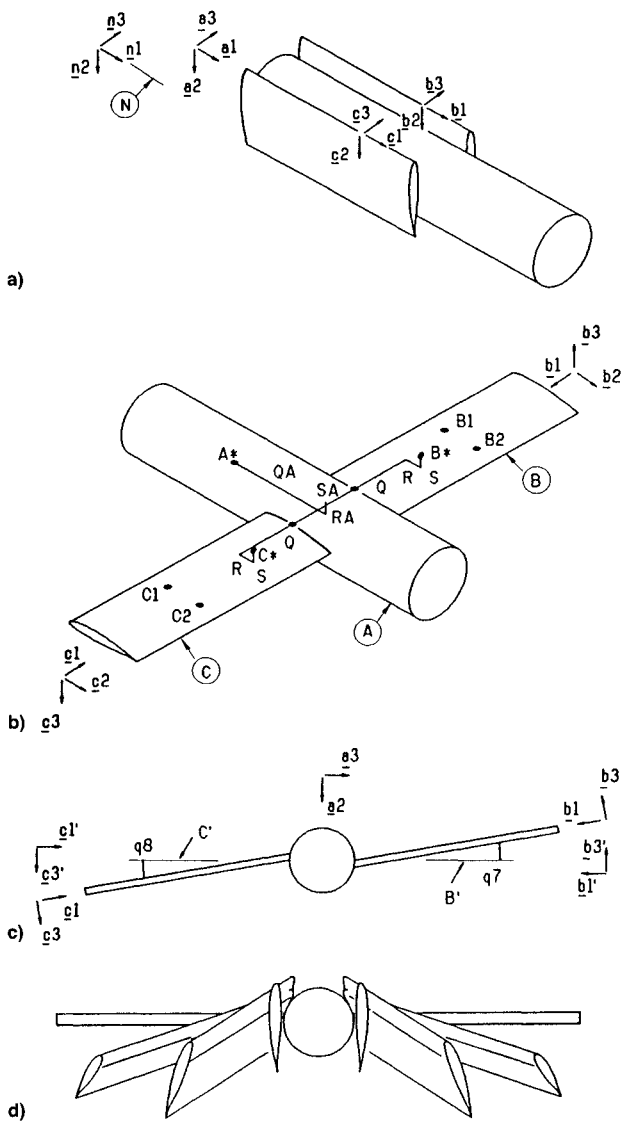

Fig. 2 LD configuration.

tions of motion and simulation codes used to predict the motion of the aircraft.

Now, writing the equations of motion, one comes to grips with the fact that, when the wings B and C are locked in their deployed configuration, the number of degrees of freedom (DOF) of S, and, consequently, the number of equations of motion, decreases. Recognizing the locking process as one of imposition of constraints,[9] one has, for the purpose of generating one, coherent simulation code, to relate variables (i.e., generalized coordinates and generalized speeds) in the equations governing the motion prior to the imposition to variables in the equations governing the motion after imposition has been completed. Current theories dealing with such situations involve the introduction of compliances in the surfaces of mechanical parts in which physical contact occurs during the imposition.[10] These compliances are introduced when certain kinematical conditions are met, and thus, the number of dynamical equations remains unchanged. The presence of such compliances, however, may lead to numerical problems in the integration, as pointed out, e.g., by Fassler.[11] The analysis at hand is particularly susceptible to such problems, because the duration of a typical mission significantly exceeds the duration of the deployment process, so that numerical problems may be carried along most of the integration time. Hence, one should attempt to integrate as simple and problem-free equations as possible, i.e., the ones governing the motion after deployment had been completed.

This article deals first with the generation of simulation codes, a task undertaken in the section on Equations of Motion. A comparison between a code based on the theory of imposition of constraints, introduced in the section on Imposition of Constraints, and a code involving compliances, is carried out in the section on Simulation Codes for UD configuration. An analysis of the behavior of the two indicated aircraft configurations is presented in the section on Deployment Simulations, and conclusions are drawn in the final section.

Equations of Motion

If the flexibility of B and C is modeled by torsion springs connecting B and C to their respective axes, then the aircraft comprises a system of 10 DOF. Ten generalized speeds are needed to describe the motion of S in N. The first six of these may be defined as follows:

$$u_r \triangleq {}^N\boldsymbol{\omega}^A \cdot \boldsymbol{a}_r \qquad (r = 1, 2, 3) \tag{6}$$

$$u_{3+r} \triangleq {}^N\boldsymbol{v}^{A^*} \cdot \boldsymbol{n}_r \qquad (r = 1, 2, 3) \tag{7}$$

where ${}^N\boldsymbol{\omega}^A$ and ${}^N\boldsymbol{v}^{A^*}$ are, respectively, the angular velocity of A in N, and the velocity of A^* in N. The four last generalized speeds can be defined with the aid of two additional reference frames B' and C', defined so that $\boldsymbol{\lambda}_{BU}$ and $\boldsymbol{\lambda}_{CU}$ are fixed both in A and in B' and C', respectively; B' is rotated about $\boldsymbol{\lambda}_{BU}$ an amount q_9 in A, and C' is rotated about $\boldsymbol{\lambda}_{CU}$

an amount q_{10} in A. Moreover, two sets of three, mutually perpendicular unit vectors $\boldsymbol{b}_i'$ and $\boldsymbol{c}_i'$ $(i = 1, 2, 3)$ fixed in B' and C', are defined so that when $q_9 = 0$, $\boldsymbol{b}_i'$ coincide with $\boldsymbol{a}_i$, and when $q_{10} = 0$, $\boldsymbol{c}_i'$ coincide with $\boldsymbol{a}_i$ $(i = 1, 2, 3)$; and when q_7, the angular deflection of the spring attached to B, equals zero, $\boldsymbol{b}_i$ coincide with $\boldsymbol{b}_i'$, and, similarly, when q_8, the angular deflection of the spring attached to C, equals zero, $\boldsymbol{c}_i$ coincide with $\boldsymbol{c}_i'$ $(i = 1, 2, 3)$. Accordingly, Eqs. (1) and (4) are replaced with

$$\boldsymbol{\lambda}_{BU} = (1/\sqrt{3})(-\boldsymbol{b}_1' - \boldsymbol{b}_2' - \boldsymbol{b}_3') \tag{8}$$

$$\boldsymbol{\lambda}_{CU} = (1/\sqrt{3})(-\boldsymbol{c}_1' - \boldsymbol{c}_2' + \boldsymbol{c}_3') \tag{9}$$

and, with self-explanatory notation, u_7, u_8, u_9, and u_{10} can be defined as

$$u_7 \triangleq {}^{B'}\boldsymbol{\omega}^{B} \cdot \boldsymbol{b}_2 \tag{10}$$

$$u_8 \triangleq {}^{C'}\boldsymbol{\omega}^{C} \cdot \boldsymbol{c}_2 \tag{11}$$

$$u_9 \triangleq {}^{A}\boldsymbol{\omega}^{B'} \cdot \boldsymbol{\lambda}_{BU} \tag{12}$$

$$u_{10} \triangleq {}^{A}\boldsymbol{\omega}^{C'} \cdot \boldsymbol{\lambda}_{CU} \tag{13}$$

where

$$\dot{q}_i = u_i \qquad (i = 7, 8, 9, 10) \tag{14}$$

Generalized inertia forces can be formulated after expressions for ${}^{N}\boldsymbol{\omega}^{B}$ and ${}^{N}\boldsymbol{\omega}^{C}$, the angular velocities of B and C in N, and ${}^{N}\boldsymbol{v}^{B^*}$ and ${}^{N}\boldsymbol{v}^{C^*}$, the velocities in N of B^* and C^*, the mass centers of B and C, respectively, have been derived. Now

$${}^{N}\boldsymbol{\omega}^{B} = {}^{N}\boldsymbol{\gamma}^{A} + {}^{A}\boldsymbol{\omega}^{B'} + {}^{B'}\boldsymbol{\omega}^{B} \tag{15}$$

$${}^{N}\boldsymbol{\omega}^{C} = {}^{N}\boldsymbol{\omega}^{A} + {}^{A}\boldsymbol{\omega}^{C'} + {}^{C'}\boldsymbol{\omega}^{C} \tag{16}$$

so that, with

$${}^{N}\boldsymbol{\omega}^{A} = u_1\boldsymbol{a}_1 + u_2\boldsymbol{a}_2 + u_3\boldsymbol{a}_3 \tag{17}$$

$${}^{A}\boldsymbol{\omega}^{B'} = u_9\boldsymbol{\lambda}_{BU}, \qquad {}^{A}\boldsymbol{\omega}^{C'} = -u_{10}\boldsymbol{\lambda}_{CU} \tag{18}$$

$${}^{B'}\boldsymbol{\omega}^{B} = u_7\boldsymbol{b}_2, \qquad {}^{C'}\boldsymbol{\omega}^{C} = u_8\boldsymbol{c}_2 \tag{19}$$

obtainable from Eqs. (6) and (10–13), expressions for ${}^{N}\boldsymbol{\omega}^{B}$ and ${}^{N}\boldsymbol{\omega}^{C}$ are readily available. Next, let $\tilde{B}$ and $\tilde{C}$ be any points on the axes of B' in A and C' in A, respectively, and let $\boldsymbol{p}^{A^*/\tilde{B}}$, $\boldsymbol{p}^{A^*/\tilde{C}}$, $\boldsymbol{p}^{\tilde{B}/B^*}$, and $\boldsymbol{p}^{\tilde{C}/C^*}$ be the position vectors from A^* to $\tilde{B}$, from A^* to $\tilde{C}$, from $\tilde{B}$ to B^*, and from $\tilde{C}$ to C^*, respectively, expressed as

$$\boldsymbol{p}^{A^*/\tilde{B}} = QA\boldsymbol{a}_1 + RA\boldsymbol{a}_2 - SA\boldsymbol{a}_3 \tag{20}$$

$$\boldsymbol{p}^{A^*/\tilde{C}} = QA\boldsymbol{a}_1 + RA\boldsymbol{a}_2 + SA\boldsymbol{a}_3 \tag{21}$$

$$\boldsymbol{p}^{\tilde{B}/B^*} = -Q\boldsymbol{b}_1 + R\boldsymbol{b}_2 + S\boldsymbol{b}_3 \tag{22}$$

$$\boldsymbol{p}^{\tilde{C}/C^*} = -Q\boldsymbol{c}_1 + R\boldsymbol{c}_2 + S\boldsymbol{c}_3 \tag{23}$$

where QA, RA, SA, Q, R, and S are shown in Fig. 1. Then, with Eq. (7)

$${}^{N}\boldsymbol{v}^{A^*} = u_4\boldsymbol{n}_1 + u_5\boldsymbol{n}_2 + u_6\boldsymbol{n}_3 \tag{24}$$

$${}^{N}\boldsymbol{v}^{B} = {}^{N}\boldsymbol{v}^{A^*} + {}^{N}\boldsymbol{\omega}^{A} \times \boldsymbol{p}^{A^*/\tilde{B}} \tag{25}$$

$${}^{N}\boldsymbol{v}^{C} = {}^{N}\boldsymbol{v}^{A^*} + {}^{N}\boldsymbol{\omega}^{A} \times \boldsymbol{p}^{A^*/\tilde{C}} \tag{26}$$

$${}^{N}\boldsymbol{v}^{B^*} = {}^{N}\boldsymbol{v}^{B} + {}^{N}\boldsymbol{\omega}^{B} \times \boldsymbol{p}^{\tilde{B}/B^*} \tag{27}$$

$${}^{N}\boldsymbol{v}^{C^*} = {}^{N}\boldsymbol{v}^{C} + {}^{N}\boldsymbol{\omega}^{C} \times \boldsymbol{p}^{\tilde{C}/C^*} \tag{28}$$

Substitutions in Eqs. (15), (16), (27), and (28) lead, after defining direction cosines between each two of $\boldsymbol{n}_i$, $\boldsymbol{a}_i$, $\boldsymbol{b}_i'$, and $\boldsymbol{b}_i$, $(i = 1, 2, 3)$, and between each two of $\boldsymbol{n}_i$, $\boldsymbol{a}_i$, $\boldsymbol{c}_i'$, and $\boldsymbol{c}_i$, $(i = 1, 2, 3)$, to the desirable expressions for ${}^{N}\boldsymbol{\omega}^{B}$, ${}^{N}\boldsymbol{\omega}^{C}$, ${}^{N}\boldsymbol{v}^{B^*}$, and ${}^{N}\boldsymbol{v}^{C^*}$. These, together with ${}^{N}\boldsymbol{\omega}^{A}$ and ${}^{N}\boldsymbol{v}^{A^*}$ in Eqs. (17) and (24), serve in deriving inertia forces, on the one hand, and in identifying partial angular velocities and partial velocities, on the other. Kane's formulation[12] can now be applied, leading to expressions for generalized inertia forces.

The active forces and torques exerted on S are as follows:

1) Torques due to torsional springs and dampers connecting B and C to their respective axes. These can be expressed

$$\boldsymbol{T}^{B'/B} = -(K_B q_7 + B_B u_7)\boldsymbol{b}_2 \tag{29}$$

$$\boldsymbol{T}^{C'/C} = -(K_C q_8 + B_C u_8)\boldsymbol{c}_2 \tag{30}$$

where K_B and K_C are the rates of the respective springs, having numerical values that represent the elasticity of the wings; and B_B and B_C are constants representing the structural damping of the wings.

2) Gravitational forces, which, with self-explanatory notation, take the form

$$\boldsymbol{F}^{A^*} = -m_A g\underline{n}_2, \qquad \boldsymbol{F}^{B^*} = -m_B g\underline{n}_2, \qquad \boldsymbol{F}^{C^*} = -m_C g\boldsymbol{n}_2 \tag{31}$$

where m_A, m_B, and m_C are, respectively, the masses of A, B, and C, and g is the gravitational acceleration.

3) Aerodynamical forces and torques, expressed in terms of ρ, the air density; v_i $(i = 1, 2, 3)$, the $\boldsymbol{b}_i$ or $\boldsymbol{c}_i$ components of the velocity of control points of B or C with respect to the air; S_W, the wing area; AR_W, the ratio between the span and the width of the wing; l_R, a reference length; α, the attack angle calculated at the respective control point; and $C_L(\alpha)$, C_{NL}, $C_M(\alpha)$, and C_A, lift coefficients. Written for B, these forces and torques are

3-1 linear lift force at B_1

$$\boldsymbol{Z}_L^{B_1} = \tfrac{1}{4}\rho(v_1^2 + v_2^2)S_W C_L(\alpha)\{1/[1 + (2/AR_W)]\}\boldsymbol{b}_3 \tag{32}$$

where B_1 is a control point on B (see Fig. 1b).

3-2 nonlinear lift force at B_2

$$\boldsymbol{Z}_{NL}^{B_2} = \tfrac{1}{4}\rho v_3^2 S_W C_{NL}\,\mathrm{sign}(v_3)\boldsymbol{b}_3 \tag{33}$$

where B_2 is a control point on B (see Fig. 1b).

3-3 pitch torque for B^*

$$\boldsymbol{M}^{B} = -\tfrac{1}{4}\rho(v_1^2 + v_3^2)S_W C_M(\alpha)\{1/[1 + (2/AR_W)]\}\boldsymbol{b}_1 \tag{34}$$

3-4 in-plane drag force at B_2

$$\boldsymbol{A}^{B_2} = \tfrac{1}{4}\rho v_1^2 S_W C_A\,\mathrm{sign}(v_1)\boldsymbol{b}_2 \tag{35}$$

Similar expressions can be written for C, with $-\boldsymbol{c}_3$ replacing $\boldsymbol{b}_3$ in Eqs. (32) and (33), with $\boldsymbol{c}_1$ and $\boldsymbol{c}_2$ replacing $\boldsymbol{b}_1$ and $\boldsymbol{b}_2$ in Eqs. (34) and (35), respectively, and with C_1 and C_2 as control points replacing B_1 and B_2. The attack angle α at a control point is defined

$$\begin{aligned} \alpha &\triangleq \tan^{-1}(v_3/v_1) \qquad 0 < v_1 \\ \alpha &\triangleq 180 - \tan^{-1}(v_3/v_1) \qquad 0 < v_1 \end{aligned} \tag{36}$$

When the velocities in N of B_1, B_2, C_1, and C_2 are derived, contributions of the active forces in Eqs. (29–35) to the generalized active forces can be obtained. Substitutions of the generalized active forces and the generalized inertia forces in

Kane's equations,[12] lead directly to a set of equations governing the motion of S in N prior to the locking of the wings. In the present work these equations were derived and coded for UD and LD configurations with the aid of Autolev, an interactive, symbol manipulation program for analyzing the dynamics of mechanical systems.[13]

Imposition of Constraints

Suppose B is the first to complete its deployment and is locked to the fuselage. Then $u_9 = 0$, and S becomes a system of nine DOF. Similarly, when C completes deployment, then $u_{10} = 0$, and S becomes a system of only eight DOF. With

$$u_9 = 0, \qquad u_{10} = 0 \tag{37}$$

as motion constraints imposed on S, one at a time, one can obtain equations governing the motion of S in N 1) by invoking the theory of imposition of constraints stated below, and 2) by assuming that when q_9 and q_{10} reach 120 deg, torsion springs and dampers, representing the above mentioned compliances, are activated, exerting on B and on C torques that oppose deviation of q_9 and q_{10} from 120 deg. Thus, without changing the number of degrees of freedom, one is capable of approximating the imposition of constraints. A comparison between simulations based on the two approaches will follow the introduction of the theory of imposition of constraints.[9]

Now, the idea of imposition of constraints comes to light in connection with a system S of ν particles P_i ($i = 1, \ldots, \nu$) of mass m_i possessing n generalized coordinates $q_1, \ldots, q_n$, and n generalized speeds $u_1, \ldots, u_n$ in N, undergoing three phases of motion, as follows: Phase a occurs in the time interval $0 \leq t < t_1$. The motion of S in N is unconstrained, and governed by n dynamical equations, viz.,

$$F_r + F_r^* = 0 \qquad (r = 1, \ldots, n) \tag{38}$$

where F_r and F_r^* are the rth generalized active force and the rth generalized inertia force, respectively. Phase b occurs in the time interval $t_1 \leq t \leq t_2$, where $t_2 - t_1$ is "small," say, compared to time constants associated with the motion of S. Then, m constraints of the form

$$u_k = \sum_{r=1}^{p} C_{kr} u_r + D_k \qquad (k = p + 1, \ldots, n) \tag{39}$$

are imposed on S, where

$$p \triangleq n - m \tag{40}$$

and C_{kr} and D_k are functions of $q_1, \ldots, q_n$ and time t. In this phase, the configuration of S in N remains unaltered, i.e.,

$$q_r(t_2) = q_r(t_1) \qquad (r = 1, \ldots, n) \tag{41}$$

and the number of independent, generalized speeds is reduced from n to p. The relation between $u_k(t_2)$ ($k = p + 1, \ldots, n$), the values of the dependent generalized speeds at $t = t_2$, and $u_r(t_2)$ ($r = 1, \ldots, p$), the values of the independent generalized speeds at $t = t_2$ is given by

$$u_k(t_2) = \sum_{r=1}^{p} C_{kr} u_r(t_2) + D_k \qquad (k = p + 1, \ldots, n) \tag{42}$$

Additionally, the relation between $u_s(t_2)$ ($s = 1, \ldots, n$) and $u_s(t_1)$ ($s = 1, \ldots, n$) is given by

$$\sum_{s=1}^{n} \left(m_{rs} + \sum_{k=p+1}^{n} C_{kr} m_{ks} \right) [u_s(t_2) - u_s(t_1)] = 0$$
$$(r = 1, \ldots, p) \tag{43}$$

where, with $\boldsymbol{v}^{Pi}$ as the velocity of P_i in N, m_{rs} is defined

$$m_{rs} \triangleq \sum_{i=1}^{\nu} m_i \frac{\partial \boldsymbol{v}^{Pi}}{\partial u_r} \cdot \frac{\partial \boldsymbol{v}^{Pi}}{\partial u_s} \tag{44}$$

and where C_{kr}, D_k, and m_{rs} are evaluated at t_1. Phase c occurs when $t > t_2$. Then the motion of S in N is constrained and governed by p dynamical equations, viz.,

$$F_r + F_r^* + \sum_{k=p+1}^{n} C_{kr}(F_k + F_k^*) = 0 \qquad (r = 1, \ldots, p) \tag{45}$$

Simulation Codes for UD Configuration

Two codes were built for simulating motions of systems having a UD configuration. One code, called UDI, is based on Eqs. (38–45), where the theory of imposition of constraint is used. The other, called UDS, is based on Eq. (38) (Kane's equation) with $n = 10$, where springs of rate K_S and dampers of constant B_S are activated when $q_9 = 120$ deg, such that

$$\boldsymbol{T}^{A/B'} = [-K_S(q_9 - \theta) + B_S u_9]\boldsymbol{\lambda}_{BU} \tag{46}$$

$$\boldsymbol{T}^{A/C''} = [-K_S(q_{10} - \theta) + B_S u_{10}]\boldsymbol{\lambda}_{CU} \tag{47}$$

Here, $\boldsymbol{T}^{A/B'}$ and $\boldsymbol{T}^{A/C''}$ are the torques exerted by A on B' and C', respectively.

The indicated codes were run on a 33 MHz, 486 PC with a Kutta Merson integrator. An aircraft with parameters having the following numerical values was considered: $I_{A1} = 0.007$, $I_{A2} = I_{A3} = 0.3$, $I_{B1} = I_{C1} = 0.0001$, $I_{B2} = I_{C2} = 0.0015$, $I_{B3} = I_{C3} = 0.0016$ kg-m-s^2; $A = 2$, $B = C = 0.05$ kg-m^{-1}-s^2; $K_B = K_C = 100$ kg-m/rad; and $QA = 0.24$, $RA = 0.016$, $SA = 0.08$, $Q = 0.4$, $R = -0.004$, $S = 0$ m. The aircraft was initially oriented at 45-deg to the horizon, had a mass center initial velocity of ${}^N\boldsymbol{v}^{A^*} = -20\boldsymbol{n}_1 + 20\boldsymbol{n}_2$ m/s, and was subjected to a side wind having a velocity of ${}^N\boldsymbol{v}^W = 10\underline{n}_3$ m/s. The motion was simulated with the aid of UDI code and of UDS code, yielding Figs. 3 and 4. The former involves no damping, i.e., $B_B = B_C = B_S = 0$; whereas the latter involves damping such that, with ξ as the damping ratio and with $I = (I_{B1} + I_{B2} + I_{B3})/3$, B_B, B_C, and B_S are given by $B_B = \sqrt{K_B B Q^2}\xi$, $B_C = B_B$ and $B_S = 2\sqrt{K_S I}\xi$, where $\xi = 0.01$. One may conclude that the higher the K_S, the better the fit between curves obtained with the UDS code and the curve obtained with the UDI code, and that the presence of damping does not alter this tendency.

One may then wonder why bother with the imposition of constraints theory. The answer is in Tables 1 and 2. The former shows that the time it takes to simulate 1-s real time becomes prohibitively longer as K_S increases; whereas the latter indicates that the relative efficiency of the codes remains unaltered in the presence of damping. In addition, Figs. 3 and 4 show that the reliability of UDS code decreases with t, the time through which the system behavior is simulated. Thus, UDI is recommended for simulations where postdeployment behavior is important.

A detail of interest can be observed in Figs. 3 and 4, viz., the 30-Hz oscillations in the roll angle. Such oscillations can also be observed in the time histories of other variables (Figs.

Table 1 Simulations run-time with $\xi = 0$

Code	K_S, kg-m/rad	Run-time, min
UDI	—	2:15
UDS	1,440	9:00
UDS	14,400	23:00

Table 2 Simulations run-time with K_S = 1440 kg-m/rad

Code	ξ	B_B, B_C, kg-m-s/rad	B_S, kg-m-s/rad)	Run-time, min
UDS	0	0	0	9:00
UDS	0.001	1.80	0.78	8:30
UDS	0.01	18.0	7.8	6:10
UDS	0.1	180	78	2:50
UDI	0	0	—	2:15
UDI	0.001	1.80	—	2:10
UDI	0.01	18.0	—	1:45
UDI	0.1	180	—	1:00

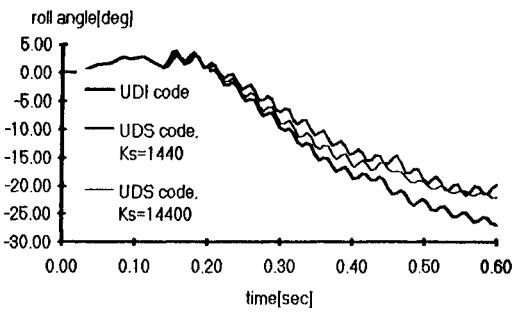

Fig. 3 Roll angle with ξ = 0.

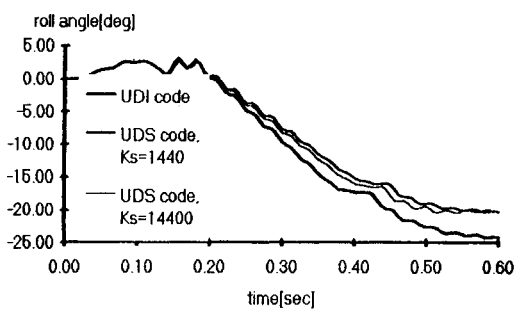

Fig. 4 Roll angle with ξ = 0.01.

5–10); and are a manifestation of the beating phenomenon,[14] resulting from the structure of the aircraft. With f_1 and f_2 as the nonzero natural frequencies associated with the aircraft after deployment, the beating phenomenon gives rise to new system frequencies, viz., $\frac{1}{2}(f_2 + f_1)$ and $\frac{1}{2}(f_2 - f_1)$. Here $f_1 = (1/2\pi)\{K/[(SA + Q)QB + I_{B2}]\}^{1/2} = 15.1$ Hz and $f_2 = f_1\{1 + 2[(SA + Q)^2B + I_{B2}]/I_{A1}\}^{1/2} = 32.8$ Hz.

One significant flaw is embedded in the theory of imposition of constraints and consequently, in the UDI code. The imposition of constraints process, having the characteristics of an impact, gives rise to "instantaneous" change in generalized speeds, shown, e.g., in Fig. 5. (Note that, with the indicated side wind, different aerodynamical loads are experienced by wings B and C, leading to termination of deployments at t = 0.138 and at t = 0.432 s, respectively). The associated infinitely large accelerations make it impossible to calculate constraint torques during the imposition.

Alternatively, UDI code can be used to predict ΔU, the total reduction in the system's energy during imposition. For example, Table 3 shows ΔU, obtained with UDI and with UDS codes for different K_S, while, with a side wind as before, wing C terminates deployment and is locked to the fuselage. Again, the results obtained with the UDS code approach those obtained with the UDI code. One may conclude that simulations obtained with the UDI code are both faster and, with unknown compliance characteristics, more accurate than those obtained with the UDS code.

Table 3 Energy loss during imposition

Code	K_S, kg-m/rad	ΔU, kg-m
UDI	—	1.25
UDS	1,440	1.25
UDS	14,400	1.24

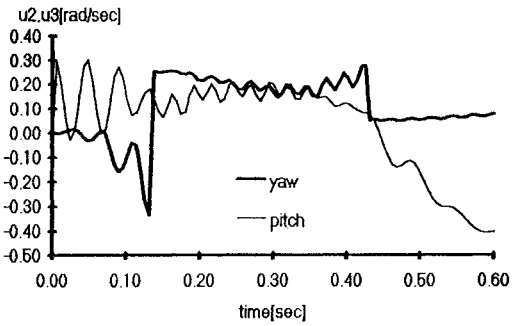

Fig. 5 Yaw and pitch rates.

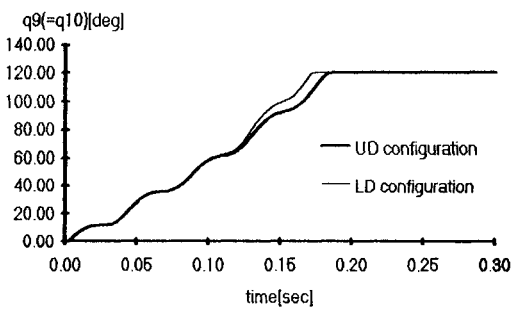

Fig. 6 Symmetric deployment.

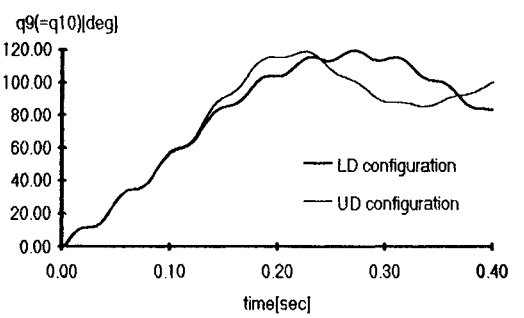

Fig. 7 Incomplete deployment.

Deployment Simulations

A code similar to UDI was constructed with reference to the LD configuration, and called LDI. A comparative study of the behavior of UD configuration and LD configuration was then carried out. In the absence of external winds and damping, $q_9(t) = q_{10}(t)$, and the two configurations give rise to similar $q_9(t)$ behavior, as shown in Fig. 6. However, this similarity disappears in the presence of external winds. For example, with the same ${}^N\boldsymbol{v}^{A^*}$ as before, an external wind of ${}^N\boldsymbol{v}^W = 5\boldsymbol{n}_1$ m/s does not enable termination of the deployment in the UD configuration (an external wind of ${}^N\boldsymbol{v}^W = -5\boldsymbol{n}_1$ m/s accelerates the deployment). A ${}^N\boldsymbol{v}^W = -11\boldsymbol{n}_1$ m/s is required in order to cause a similar effect with the LD configuration. Plots of $q_9(t)$ and $q_{10}(t)$ for these incomplete deployments are shown in Fig. 7.

Next, let the UD configuration be subjected to a side wind of ${}^N\boldsymbol{v}^W = 10\boldsymbol{n}_3$ m/s, and the LD configuration be subjected

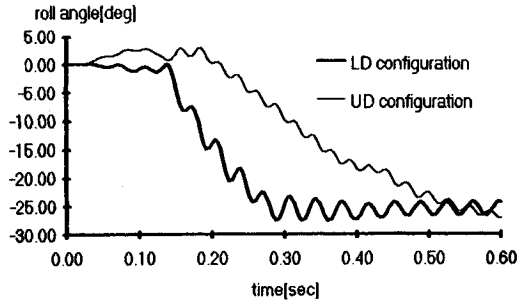

Fig. 8 Roll angle with side winds of 10 m/s.

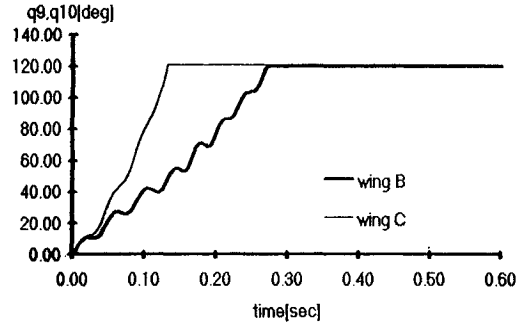

Fig. 9 UD configuration deployment with side wind of 10 m/s.

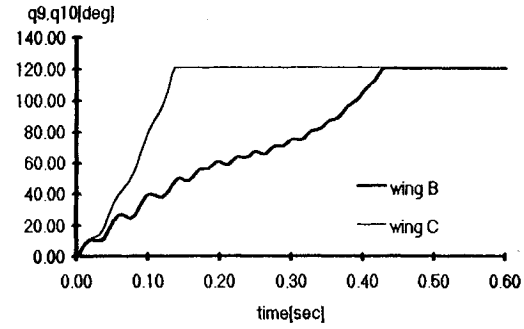

Fig. 10 LD configuration deployment with side wind of 10 m/s.

to a side wind of ${}^N\boldsymbol{v}^W = -10\boldsymbol{n}_3$ m/s. Figure 8 shows that, under these circumstances, the roll undergone by the fuselage is similar in both configurations. However, Figs. 9 and 10 indicate that it takes the UD configuration a longer time to complete deployment. Furthermore, the time the aircraft moves with only one wing locked is twice as long with the UD configuration. These results point towards a greater susceptibility of the UD configuration to wind gusts.

Thus, one may conclude that the LD configuration is less susceptible to external winds. This relative robustness has its price, because with LD configuration, ΔU is larger during the imposition phase: in the absence of external winds $\Delta U = 2.25$ kg-m with the LD configuration, and 0.7 kg-m with the UD configuration. These results indicate that a higher amount of energy must be absorbed during imposition of constraints with the LD configuration, possibly accompanied by higher loads at the roots of the wings. Robustness, however, is usually a prevailing consideration, pointing towards the LD configuration as advantageous.

Conclusions and Future Work

The matter of choosing between two acceptable configurations of axes for aerodynamically deployed wings was investigated in this article. Simulations of the deployment process for both configurations were used as tools by means of which the indicated choice could be made. In writing the requisite simulations, however, one has to deal with the loss of a DOF, occurring when the deployment of a wing terminates. The common practice in such situations is to add compliances to surfaces at which impacts occur, thus leaving the number of DOF unaltered. Such solutions lead, at best, to time-consuming simulations, a problem alleviated here with the aid of the theory of imposition of constraints. If, however, information regarding the compliance at the indicated surfaces is available, then the theory of imposition of constraint can be applied after transients, associated with the impact occurring when the deployment terminates, have died out.

With simulations capable of handling the termination of deployment, one is in a position to further investigate the UD and the LD configurations. The following issues can be investigated: To what extent does the presence of an on-board, launching power source affect the robustness of the UD configuration? What is the latest point in time for control activation, so as to avoid the aircraft loss of stability in adverse weather conditions? Is it necessary to use dampers as means to reduce the loads associated with the imposition? How effective is the available structural damping in restraining the elastic deformations and stresses resulting from the imposition?

Upgrading the codes described here may put one in a position to relate to more complex issues. Thus, if each wing is represented by either a larger number of rigid bodies, springs and dampers, or, alternatively, by a continuous or a discretized elastic media (modal representation), then it becomes possible to investigate aeroelastic stability. Similarly, the model of the aircraft can be upgraded to include additional, possibly deployable, aerodynamic surfaces, as decreed by the aerodynamic design. Control torques can also be added, eventually leading to a more comprehensive study of the aircraft launch-deploy behavior. With the imposition of constraints theory, however, a study of the launch-deploy phase of the type of aircraft in question can be accomplished without having to assume anything about the locking mechanisms of deployable members.

References

[1]Hoppner, H. J., Sparz, H., and Sadowski, H., "Unmanned Aircraft," U.S. Patent No. 4471923, Sept. 18, 1984.

[2]Crossfield, P. M., "Missile Appendage Deployment Mechanism," U.S. Patent No. 4664339, May 12, 1987.

[3]Schnäbele, W., Buckley, J., and Rieger, U., "Drone-Type Missile," U.S. Patent No. 4296894, Oct. 27, 1981.

[4]Cook, N., "Dornier, MBB Await DAR (Drohne Anti-Radar) Decision," *Jane's Defence Weekly*, Vol. 9, No. 25, June 1988, p. 1283.

[5]Taylor, J. W. R., "Jane's All the World's Aircraft Supplement," *Air Force Magazine*, Vol. 68, No. 2, Feb. 1985, p. 109.

[6]Hawley, W. W., and Haykin, D. J., "Folding Fin," U.S. Patent No. 3063375, Nov. 13, 1962.

[7]Jacot, A. D., and Hellmers, D. E., "Control Dynamics of the Deployable Wing Cruise Ballistic Missile," AIAA Paper 82-0181, Jan. 1982.

[8]Kane, T. R., Likins, P. W., and Levinson, D. A., *Spacecraft Dynamics*, McGraw-Hill, New York, 1983.

[9]Djerassi, S., "Imposition of Constraints," *Journal of Applied Mechanics*, Vol. 61, No. 2, June 1994.

[10]Mills, J. K., and Nguyen, C. V., "Robotic Manipulator Collisions: Modelling and Simulation," *Journal of Dynamic Systems, Measurement, and Control*, Vol. 114, Dec. 1992, pp. 650–659.

[11]Fassler, H., "Manipulator Constrained by Stiff Contact: Dynamics, Control and Experiments," *The International Journal of Robotics Research*, Vol. 9, No. 4, 1990, pp. 40–58.

[12]Kane, T. R., and Levinson, D. A., *Dynamics, Theory and Application*, McGraw-Hill, New York, 1985.

[13]Schaechter, D. B., Levinson, D. A., and Kane, T. R., *Autolev User's Manual*, On-Line Dynamics, Inc., Sunnyvale, CA, 1991.

[14]Thomson, W. T., *Theory of Vibration with Application*, Prentice-Hall, Englewood Cliffs, NJ, 1988.